Mon. Not. R. Astron. Soc. **000**, 1–10 (2014) Printed 24 June 2014 (MN LATEX style file v2.2)

# Flicker noise pulsar radio spectra

K. Krzeszowski,[1] O. Maron,[1] A. Słowikowska[1] and A. Jessner[2]
[1]*Kepler Institute of Astronomy, University of Zielona Góra, Lubuska 2, 65–265, Zielona Góra, Poland*
[2]*Max-Planck-Institut für Radioastronomie, Auf dem Hügel 69, D-53121 Bonn, Germany*

arXiv:1406.5584v1 [astro-ph.SR] 21 Jun 2014

Released 2014

**ABSTRACT**

We present new results of fitting 108 spectra of radio pulsars with the flicker noise model proposed by Löhmer et al. (2008) and compare them with the spectral indices of power–law fits published by Maron et al. (2000). The fits to the model were carried out using the Markov chain Monte Carlo (MCMC) method appropriate for the non–linear fits. Our main conclusion is that pulsar radio spectra can be statistically very well described by the flicker noise model over wide frequency range from a few tens of MHz up to tens of GHz. Moreover, our dataset allows us to conduct statistical analysis of the model parameters. As our results show, there is a strong negative correlation between the flicker noise spectrum model parameters $\log S_0$ and $n$ and a strong positive relationship between $n$ and the power–law spectral index $\alpha$. The latter implies that their physical meaning is similar, however the flicker noise model has an advantage over broken power–law model. Not only it describes the spectra in higher frequency range with only two parameters, not counting scaling factor $S_0$, but also it shows smooth transition from flat to steep behaviour at lower and higher frequencies, respectively. On the other hand, there are no correlations of the flicker noise model parameters $S_0$, $\tau$ and $n$ with any of pulsar physical properties.

**Key words:** pulsars: general

## 1 INTRODUCTION

Spectra of radio pulsars have been a subject of studies for many years. It is a generally accepted fact, that the pulsar radio spectra are steep and approximately follow a power-law relation: $S_\nu \sim \nu^\alpha$, where $S_\nu$ is the observed flux density at frequency $\nu$, and $\alpha$ is the spectral index.

Many studies have been carried out on the measurements of flux densities in a wide frequency range over the past years (e.g. Sieber 1973; Malofeev et al. 1994; Seiradakis et al. 1995; Lorimer et al. 1995; Maron et al. 2000). However, the first systematic study of spectral indices for a large number of pulsars was conducted by Lorimer et al. (1995) who published a catalogue of spectral indices for 280 pulsars based on observations made with the Lovell radio telescope at frequencies 0.4–1.6 GHz. More recent work by Maron et al. (2000) extended the frequency range for many cases up to 5 GHz and derived the spectral index value of $\alpha = -1.8 \pm 0.2$. They also found that in their sample $\sim 10\%$ of pulsars have double power law (broken power law) type spectrum which is described by two parameters, $\alpha_1$ at lower frequencies and $\alpha_2$ at higher frequencies. Additionally, Maron et al. (2000) discovered that PSRs B1823-13 and B1838-04 show high-frequency turnovers in their spectra. While turnovers are often observed at frequencies around and below 100 MHz (Izvekova et al. 1981), the occurrence of such an effect at frequency $\sim$ 1GHz is unusual.

In this paper we are investigating the flicker noise model proposed by Löhmer et al. (2008) where the received radio flux density is given by

$$\mathrm{S}(\omega) = \mathrm{S}_0 \left( \frac{1+\omega^2\tau^2}{\tau^2} \right)^{\mathrm{n}-1} \times \mathrm{e}^{-\mathrm{i}(\mathrm{n}-1)\mathrm{atan}(\omega\tau)}, \quad (1)$$

where $S_0$ is a scaling factor, $\omega = 2\pi\nu$, $\nu$ is an observing frequency, $\tau$ is the characteristic life time of nano bursts and $n$ is the exponent that captures a number of physical and observational properties of the emission (Löhmer et al. 2008). Pulsar fluxes and hence the input values for pulsar spectra are commonly averaged over the pulse period and therefore represent an average over what we receive from different emission regions at different phase angles. We know that many sources have strong profile evolution which is hidden in the single flux values and it would be rather surprising if a single one parameter law can fit such a spectrum well. Nevertheless, Löhmer et al. have pointed out, that even a two parameter model for a reference radio flux and a single time scale can already provide surprisingly good fits to the spectrum with

© 2014 RAS

intuitive values for the timescales that could be interpreted as observed life times of nano pulses. If one was to assume similar conditions for the emission regions observed at different pulse phases, as one would perhaps imagine to exist in pulsars with simple one component profiles, then $n$ could have more than a heuristic meaning. Assume that we have radiation processes that are confined to flux tubes forming a layer of depth $\delta$, having a particular cross section $\sigma$ and typical separation $a$ and that these emission centres can interact destructively if they overlap, then $n = \frac{\sigma}{\pi a \delta}$. If the local plasma wavelength $\lambda_{pe}(r,\gamma) = \frac{2\pi}{\omega_{pe}(r,\gamma)}$ is the decisive scale, then $n$ would just be thickness of the emission layer or alternatively the separation of emission centres in units of plasma lengths. Our results show, that like $\tau$ the range of $n$ is constrained which points to similar conditions for the emission processes of all pulsars even when one takes the averaging over phase angles and propagation effects into account.

Section 2 covers the data selection and fitting method description. In Section 3 we discuss our findings which we summarise and conclude in Section 4.

## 2 DATASET AND FITTING METHOD

Our base dataset for the analysis consists of flux measurements of 108 pulsars. The sample was selected from a much wider dataset, containing measurements for 281 pulsars, published by Maron et al. (2000). The most important data selection criterion was the coverage of the possible widest range of frequencies — flux measurements should be available at low (<200 MHz) and high (>1 GHz) frequencies to unambiguously fit all the parts of Löhmer spectrum model. Only those pulsars that met this criterion were included in the sample. Single datasets consist of minimum of 4 up to maximum of 24 flux measurements at a number of frequencies with the mean of 8 measurements. In some of the cases the fits were not reasonable due to insufficient number of low and/or high frequency measurements or measurements that were doubtful i.e. outliers or unusually high errors. Such cases are not presented in this paper, and after collection of additional published flux measurements will be presented in the upcoming paper.

### 2.1 MCMC

The model fits according to Eq. 1 were carried out using the Markov chain Monte Carlo (MCMC) method which is a machine learning algorithm (Gelfand & Smith 1990). It is mostly used to solve optimisation problems in multidimensional spaces, although it can be used for solving much simpler problems. It is a combination of memoryless Markov process and Monte Carlo randomised algorithm. The Markov process fulfils the condition, that future state of the system depends only on its present state without a need for knowing its full history. One common example is the random walk where next position depends only on present position regardless of previous steps. The main idea behind MCMC is to construct a Markov chain in the way, that its equilibrium distribution is the distribution we want to sample. To achieve this goal a number of so called walkers randomly wander the parameter space and draw a set of samples from the original, maybe unknown, distribution. After high number of steps we sample the chain instead of sampling the original distribution.

In case of a non–linear model like a power–law, one can not use $\chi^2_{\rm red}$ as the goodness of fit estimator since determination of degrees of freedom is non trivial (Andrae et al. 2010). As the fitting procedure we used a maximum likelihood method along with Markov chain Monte Carlo using *emcee* python library (Foreman-Mackey et al. 2012).

The fitting procedure was run on datasets consisting of measured values of observing frequency, flux and flux error. The MCMC algorithm in connection with the maximum likelihood estimation (MLE) allowed us to sample the $\mathbb{R}^3$ parameter space sufficiently to get smooth parameter distributions. We took the median ($50^{\rm th}$ percentile) of the resulting distributions of each parameter as parameter values as well as $16^{\rm th}$ and $84^{\rm th}$ percentiles of the distributions as a lower ($\sigma^-$) and upper ($\sigma^+$) uncertainties, respectively. For the normal distribution the 16th and 84th percentiles are equivalent of 2 sigma range and they are commonly used for error estimation.

## 3 RESULTS AND DISCUSSION

As an example of our analysis the fitted spectrum to PSR B1133+16 flux measurements is presented in Fig. 1. The same approach was taken in case of 108 sets of flux measurements for different pulsars and yielded estimations of parameters $S_0$, $\tau$ and $n$. Parameter distributions for PSR B1133+16, along with their correlations, as an example are presented in Fig. 2. The plot presents 1–D and 2–D posterior probability distributions of three fitted parameters $S_0$, $\tau$ and $n$. The most frequently occurring values for each parameter are marked with solid vertical and horizontal lines. The diagonal 1–D distributions are symmetric and Gaussian–like which is not always like this. In this case it means, that the fit is reasonable and the parameter estimations along with their errors, taken as the $16^{\rm th}$ and $84^{\rm th}$ percentile of each distribution, are precise.

Resulting parameters $S_0$, $\tau$ and $n$ for all pulsars and respective uncertainties, along with a number of flux measurements of fitting 108 spectra are gathered in Tab. 1. The table also contains spectral indices from Maron et al. (2000) of power–law fits (95 values) and high frequency parts of broken power–law fits (13 values, denoted with superscript $b$). The distributions of all fitted parameters and their upper and lower uncertainties are shown in Fig. 3. The parameters range from 0.015 Jy (B2022+50) to 14.127 Jy (B0531+21) in case of $S_0$, from 0.041 ns (B1800-21) to 2.014 ns (B2022+50) in case of $\tau$ and from 0.003 (B2000+40) to 0.544 (B2022+50) in case of $n$ with mean values of 1.197 Jy, 0.586 ns and 0.143 for $S_0$, $\tau$ and $n$, respectively. Fifty percent of $S_0$, $\tau$ and $n$ values are between 0.17–1.20 Jy, 0.25–0.84 ns and

0.07–0.20, respectively. One of the most noticeable pulsar in our sample is PSR B2022+50 (J2023+5037). It has a period of P = 0.373 s., a polarisation angle curve showing an orthogonal mode and its interpulse is 100% polarised (Han et al. 2009). Our fit of the flicker noise spectrum model to B2022+50 flux measurements yielded $S_0$ = 0.015 Jy, $\tau$ = 2.014 ns and $n$ = 0.544, which are extreme values within our whole sample. This pulsar is the weakest one so the scaling factor $S_0$ of its fit is also the smallest among all values. It is supposed to have the longest duration of nano–bursts ($\tau$) and its spectrum is not as steep as of other pulsars due to the high $n$ value.

Löhmer et al. (2008) fitted flicker noise spectra to 12 pulsars and got $S_0$, $\tau$ and $n$. In Tab. 2 we compare them with our results. Our results are consistent with previous studies except for B0144+59 and B1929+10 where $\tau$ is different by the order of magnitude. Since there are no plots or data for these pulsars in their work, we can not investigate either of the cases in details.

We also looked for the correlations between fitted parameters $S_0$, $\tau$ and $n$ and found a relationship between $S_0$ and $n$ with Pearson's correlation index of -0.52 with the 95% confidence interval of (-0.65, -0.37) and the p–value of $5.53 \times 10^{-9}$. Remaining parameters show only weak correlations, as it can be seen in Fig. 4. In the diagonal of this figure the approximated kernel densities of parameter distributions are plotted. The main pulsar radio spectrum model fitted in Maron et al. (2000) was a power–law with the mean value of spectral index $\alpha = -1.8 \pm 0.2$. Correlations of $S_0$, $\tau$ and $n$ acquired in this study with spectral indices $\alpha$ from fits of single power–law are presented in Fig. 5. There are no obvious correlations between $S_0$ and $\tau$ with $\alpha$. However, there is a strong positive relationship between $n$ and $\alpha$ with Pearson's correlation index of 0.63 with the 95% confidence interval of (0.50, 0.73) and the p–value of $2.03 \times 10^{-13}$. The linear fit yields the relation $n = 0.11\ \alpha + 0.34$. This suggests that the physical interpretation of $n$ and the power–law spectral index $\alpha$ is similar. Apart from that, there are no correlations of $S_0$, $\tau$ and $n$ with any of pulsar physical parameters like period, period derivative, age, rotational energy loss, magnetic field on surface or dispersion and rotation measures.

### 3.1 PSR B1133+16

PSR B1133+16 is one of the strongest and most frequently observed pulsars. Since 2000 there were many observations which allowed us to extend the original data (19 measurements) from Maron et al. (2000) with additional 41 measurements that were gathered in Krzeszowski et al. (2014). Fig. 1 shows the results of fitting the flicker noise spectrum to PSR B1133+16 flux measurements. These data were divided into two sets: original set of points from Maron et al. (2000) marked with black filled circles and all measurements from Krzeszowski et al. (2014) marked with black filled circles and black opened circles altogether. The fits are plotted with solid line and dashed line for Maron's data and Krzeszowski's data, respectively, however both fits are indistinguishable. The spectrum is relatively flat at lower frequencies ($< 300$ MHz) and becomes steep at higher frequencies. The resulting parameters are as follows: $S_0^{\mathrm{M}} = 3.48^{+0.34}_{-0.35}$ Jy, $\tau^{\mathrm{M}} = 0.39^{+0.03}_{-0.03}$ ns, $n^{\mathrm{M}} = 0.12^{+0.01}_{-0.01}$ and $S_0^{\mathrm{K}} = 3.39^{+0.35}_{-0.32}$ Jy, $\tau^{\mathrm{K}} = 0.40^{+0.02}_{-0.02}$ ns, $n^{\mathrm{K}} = 0.12^{+0.01}_{-0.01}$, where superscripts M and K denote respective datasets. In this case it is clear that tripling the number of available data points from 19 to 60 does not alter the fit when the original data sample the frequency space sufficiently well in low and high frequency regions.

In Krzeszowski et al. (2014) we fitted Löhmer model to 60 flux measurements using the least squares method and got the following results: $S_0 = 3.39 \pm 0.77$ Jy, $\tau = 0.40 \pm 0.05$ ns, $n = 0.118 \pm 0.022$ and $\chi^2_{\mathrm{red}} = 4.7$. The model is non–linear and the obtained $\chi^2_{\mathrm{red}}$ is much greater than 1 and the error distribution is not normal, hence least squares method is not appropriate here (see Sec. 2.1). Still, the values are in good agreement with the values obtained with the MCMC, however the parameter errors from MCMC are 2–2.5 times smaller than in case of the least squares method.

Table 1: The fitted parameters ($S_0$ [Jy], $\tau$ [ns] and $n$) with their respective upper ($\sigma^+$) and lower ($\sigma^-$) uncertainties, N denotes a number of flux measurements that fit was performed on. Additionally, power–law spectral index $\alpha$ is included for reference (Maron et al. 2000). $\alpha_2$ values from broken power–law are denoted with superscript $b$.

| Pulsar | N | $S_0$ | $\sigma^+_{S_0}$ | $\sigma^-_{S_0}$ | $\tau$ | $\sigma^+_\tau$ | $\sigma^-_\tau$ | n | $\sigma^+_n$ | $\sigma^-_n$ | $\alpha$ |
|---|---|---|---|---|---|---|---|---|---|---|---|
| B0011+47 | 6 | 0.200 | 0.162 | 0.083 | 0.219 | 0.097 | 0.049 | 0.214 | 0.086 | 0.092 | -1.3 |
| B0037+56 | 7 | 0.056 | 0.007 | 0.006 | 1.096 | 0.302 | 0.224 | 0.193 | 0.017 | 0.017 | -1.8 |
| B0052+51 | 7 | 0.170 | 0.073 | 0.047 | 0.124 | 0.019 | 0.015 | 0.077 | 0.042 | 0.043 | -0.7 |
| B0105+65 | 4 | 0.086 | 0.032 | 0.023 | 0.641 | 0.210 | 0.144 | 0.154 | 0.074 | 0.075 | -1.9 |
| B0136+57 | 11 | 0.457 | 0.049 | 0.045 | 0.219 | 0.019 | 0.016 | 0.126 | 0.013 | 0.013 | $-2.3^b$ |
| B0138+59 | 9 | 0.573 | 0.069 | 0.056 | 0.432 | 0.052 | 0.053 | 0.115 | 0.015 | 0.016 | -1.9 |
| B0144+59 | 10 | 0.024 | 0.004 | 0.004 | 1.901 | 0.718 | 0.660 | 0.415 | 0.031 | 0.031 | -1.0 |
| B0148-06 | 5 | 0.196 | 0.089 | 0.069 | 0.933 | 0.883 | 0.382 | 0.169 | 0.066 | 0.066 | -2.7 |
| B0301+19 | 9 | 0.416 | 0.211 | 0.123 | 0.298 | 0.083 | 0.063 | 0.106 | 0.062 | 0.061 | $-2.3^b$ |
| B0320+39 | 8 | 0.384 | 0.047 | 0.049 | 0.887 | 0.133 | 0.136 | 0.048 | 0.009 | 0.008 | -2.9 |
| B0329+54 | 24 | 10.085 | 0.827 | 0.852 | 0.263 | 0.014 | 0.014 | 0.077 | 0.006 | 0.006 | -2.2 |
| B0331+45 | 6 | 0.054 | 0.019 | 0.013 | 0.917 | 0.716 | 0.350 | 0.260 | 0.055 | 0.061 | -1.9 |

Continued on next page

Table 1: The fitted parameters ($S_0$ [Jy], $\tau$ [ns] and $n$) with their respective upper ($\sigma^+$) and lower ($\sigma^-$) uncertainties, N denotes a number of flux measurements that fit was performed on. Additionally, power–law spectral index $\alpha$ is included for reference (Maron et al. 2000). $\alpha_2$ values from broken power–law are denoted with superscript *b*.

| Pulsar | N | $S_0$ | $\sigma^+_{S_0}$ | $\sigma^-_{S_0}$ | $\tau$ | $\sigma^+_\tau$ | $\sigma^-_\tau$ | n | $\sigma^+_n$ | $\sigma^-_n$ | $\alpha$ |
|---|---|---|---|---|---|---|---|---|---|---|---|
| B0353+52 | 7 | 0.156 | 0.028 | 0.023 | 0.309 | 0.055 | 0.045 | 0.148 | 0.023 | 0.024 | -1.6 |
| B0355+54 | 21 | 0.689 | 0.455 | 0.246 | 0.085 | 0.041 | 0.020 | 0.398 | 0.041 | 0.052 | $-1.2^b$ |
| B0402+61 | 5 | 0.132 | 0.019 | 0.013 | 0.457 | 0.297 | 0.095 | 0.233 | 0.019 | 0.022 | -1.4 |
| B0410+69 | 5 | 0.078 | 0.011 | 0.010 | 1.220 | 0.337 | 0.245 | 0.097 | 0.020 | 0.019 | -2.4 |
| B0450+55 | 10 | 0.366 | 0.047 | 0.037 | 0.558 | 0.227 | 0.186 | 0.272 | 0.012 | 0.014 | -1.5 |
| B0458+46 | 7 | 0.241 | 0.033 | 0.027 | 0.240 | 0.018 | 0.016 | 0.094 | 0.019 | 0.020 | -1.3 |
| B0523+11 | 8 | 0.200 | 0.018 | 0.016 | 0.772 | 0.128 | 0.128 | 0.144 | 0.017 | 0.019 | -2.0 |
| B0531+21 | 6 | 14.127 | 3.408 | 2.734 | 1.631 | 0.620 | 0.438 | 0.019 | 0.012 | 0.010 | -3.1 |
| B0540+23 | 11 | 0.808 | 0.265 | 0.170 | 0.119 | 0.015 | 0.014 | 0.232 | 0.026 | 0.029 | $-1.6^b$ |
| B0626+24 | 6 | 0.255 | 0.035 | 0.030 | 1.145 | 0.533 | 0.330 | 0.206 | 0.024 | 0.024 | -1.6 |
| B0628-28 | 13 | 2.696 | 0.223 | 0.206 | 0.550 | 0.047 | 0.047 | 0.103 | 0.009 | 0.009 | -1.9 |
| B0643+80 | 6 | 0.062 | 0.014 | 0.011 | 0.526 | 0.143 | 0.116 | 0.157 | 0.029 | 0.031 | -1.9 |
| B0740-28 | 11 | 2.991 | 0.216 | 0.193 | 0.527 | 0.042 | 0.039 | 0.110 | 0.011 | 0.012 | -2.0 |
| B0809+74 | 13 | 0.998 | 0.097 | 0.099 | 1.322 | 0.160 | 0.143 | 0.211 | 0.010 | 0.010 | -1.4 |
| B0823+26 | 16 | 0.577 | 0.073 | 0.070 | 0.946 | 0.138 | 0.126 | 0.211 | 0.012 | 0.012 | $-2.1^b$ |
| B0834+06 | 11 | 1.767 | 0.141 | 0.162 | 1.032 | 0.078 | 0.072 | 0.011 | 0.007 | 0.006 | -2.7 |
| B0919+06 | 14 | 0.499 | 0.067 | 0.065 | 0.814 | 0.131 | 0.111 | 0.162 | 0.018 | 0.018 | -1.8 |
| B0950+08 | 14 | 12.619 | 0.787 | 0.842 | 0.304 | 0.022 | 0.021 | 0.061 | 0.004 | 0.004 | -2.2 |
| B1112+50 | 7 | 0.064 | 0.010 | 0.009 | 1.752 | 0.778 | 0.575 | 0.293 | 0.026 | 0.026 | -1.7 |
| B1133+16 | 19 | 3.482 | 0.342 | 0.345 | 0.393 | 0.030 | 0.028 | 0.115 | 0.008 | 0.008 | -1.9 |
| B1237+25 | 15 | 2.980 | 0.182 | 0.170 | 0.256 | 0.018 | 0.017 | 0.056 | 0.006 | 0.006 | $-2.2^b$ |
| B1508+55 | 11 | 1.431 | 0.115 | 0.103 | 0.676 | 0.054 | 0.053 | 0.054 | 0.015 | 0.015 | -2.2 |
| B1540-06 | 7 | 0.213 | 0.033 | 0.031 | 0.934 | 0.273 | 0.189 | 0.208 | 0.026 | 0.027 | -2.0 |
| B1541+09 | 8 | 1.222 | 0.071 | 0.064 | 0.540 | 0.106 | 0.120 | 0.023 | 0.006 | 0.009 | -2.6 |
| B1552-23 | 5 | 0.101 | 0.031 | 0.021 | 0.322 | 0.083 | 0.054 | 0.142 | 0.041 | 0.046 | -1.8 |
| B1604-00 | 11 | 0.467 | 0.091 | 0.078 | 0.626 | 0.102 | 0.089 | 0.143 | 0.024 | 0.025 | -1.5 |
| B1612+07 | 6 | 0.137 | 0.028 | 0.022 | 1.214 | 0.451 | 0.393 | 0.078 | 0.010 | 0.010 | -2.6 |
| B1633+24 | 5 | 0.101 | 0.013 | 0.013 | 0.851 | 0.190 | 0.165 | 0.103 | 0.022 | 0.023 | -2.4 |
| B1642-03 | 12 | 3.468 | 0.500 | 0.495 | 0.423 | 0.035 | 0.031 | 0.044 | 0.015 | 0.015 | -2.3 |
| B1702-19 | 7 | 0.145 | 0.025 | 0.022 | 1.952 | 0.682 | 0.635 | 0.333 | 0.027 | 0.026 | -1.3 |
| B1706-16 | 12 | 0.284 | 0.031 | 0.030 | 0.842 | 0.191 | 0.185 | 0.275 | 0.010 | 0.010 | -1.5 |
| B1730-22 | 4 | 0.432 | 0.069 | 0.061 | 0.358 | 0.113 | 0.062 | 0.043 | 0.018 | 0.018 | -2.0 |
| B1732-07 | 4 | 0.369 | 0.044 | 0.040 | 0.311 | 0.036 | 0.030 | 0.051 | 0.015 | 0.016 | -1.9 |
| B1737+13 | 6 | 0.209 | 0.043 | 0.032 | 0.587 | 0.110 | 0.101 | 0.199 | 0.033 | 0.037 | -1.5 |
| B1738-08 | 6 | 0.394 | 0.073 | 0.069 | 0.703 | 0.186 | 0.153 | 0.089 | 0.019 | 0.018 | -2.2 |
| B1742-30 | 6 | 0.641 | 0.089 | 0.078 | 0.363 | 0.076 | 0.051 | 0.247 | 0.021 | 0.021 | -1.6 |
| B1749-28 | 10 | 8.925 | 0.536 | 0.742 | 0.449 | 0.026 | 0.022 | 0.005 | 0.009 | 0.004 | $-4.3^b$ |
| B1750-24 | 5 | 0.095 | 0.075 | 0.037 | 0.096 | 0.020 | 0.015 | 0.261 | 0.069 | 0.078 | -1.0 |
| B1753-24 | 5 | 0.350 | 0.049 | 0.067 | 0.121 | 0.012 | 0.009 | 0.025 | 0.028 | 0.017 | -0.7 |
| B1800-21 | 7 | 3.449 | 3.494 | 1.369 | 0.041 | 0.006 | 0.005 | 0.178 | 0.055 | 0.070 | $-1.0^b$ |
| B1804-08 | 5 | 0.958 | 0.408 | 0.225 | 0.244 | 0.040 | 0.032 | 0.198 | 0.051 | 0.062 | -1.2 |
| B1811+40 | 5 | 0.104 | 0.048 | 0.029 | 0.569 | 0.233 | 0.183 | 0.165 | 0.061 | 0.070 | -1.8 |
| B1815-14 | 6 | 0.897 | 0.359 | 0.274 | 0.105 | 0.016 | 0.012 | 0.070 | 0.048 | 0.043 | -1.6 |
| B1819-22 | 6 | 0.561 | 0.054 | 0.047 | 0.245 | 0.020 | 0.019 | 0.036 | 0.014 | 0.015 | -1.7 |
| B1820-11 | 6 | 0.152 | 0.039 | 0.029 | 0.247 | 0.049 | 0.036 | 0.289 | 0.033 | 0.035 | -1.5 |
| B1822+00 | 4 | 0.119 | 0.025 | 0.025 | 0.839 | 0.342 | 0.245 | 0.060 | 0.046 | 0.038 | -2.4 |
| B1826-17 | 7 | 1.913 | 0.167 | 0.155 | 0.234 | 0.017 | 0.015 | 0.045 | 0.010 | 0.010 | -1.7 |
| B1830-08 | 5 | 0.446 | 0.441 | 0.180 | 0.088 | 0.016 | 0.015 | 0.188 | 0.067 | 0.085 | -1.1 |
| B1831-04 | 6 | 0.465 | 0.091 | 0.061 | 0.465 | 0.110 | 0.090 | 0.311 | 0.032 | 0.038 | -1.3 |

Continued on next page

Table 1: The fitted parameters ($S_0$ [Jy], $\tau$ [ns] and $n$) with their respective upper ($\sigma^+$) and lower ($\sigma^-$) uncertainties, N denotes a number of flux measurements that fit was performed on. Additionally, power–law spectral index $\alpha$ is included for reference (Maron et al. 2000). $\alpha_2$ values from broken power–law are denoted with superscript $b$.

| Pulsar | N | $S_0$ | $\sigma^+_{S_0}$ | $\sigma^-_{S_0}$ | $\tau$ | $\sigma^+_\tau$ | $\sigma^-_\tau$ | n | $\sigma^+_n$ | $\sigma^-_n$ | $\alpha$ |
|---|---|---|---|---|---|---|---|---|---|---|---|
| B1839+56 | 7 | 0.254 | 0.076 | 0.054 | 0.289 | 0.097 | 0.064 | 0.188 | 0.032 | 0.036 | -1.5 |
| B1841-04 | 6 | 0.157 | 0.052 | 0.045 | 0.267 | 0.059 | 0.034 | 0.083 | 0.061 | 0.050 | -1.6 |
| B1844-04 | 6 | 0.762 | 0.053 | 0.046 | 0.620 | 0.058 | 0.055 | 0.091 | 0.014 | 0.015 | -2.2 |
| B1846-06 | 5 | 0.323 | 0.031 | 0.027 | 0.749 | 0.151 | 0.127 | 0.080 | 0.018 | 0.020 | -2.2 |
| B1857-26 | 6 | 2.346 | 0.223 | 0.208 | 0.334 | 0.041 | 0.032 | 0.035 | 0.014 | 0.015 | -2.1 |
| B1859+03 | 6 | 3.134 | 0.510 | 0.376 | 1.229 | 0.255 | 0.204 | 0.013 | 0.006 | 0.006 | -2.8 |
| B1859+07 | 6 | 0.312 | 0.081 | 0.091 | 0.134 | 0.020 | 0.012 | 0.041 | 0.040 | 0.027 | -1.0 |
| B1900-06 | 4 | 0.317 | 0.057 | 0.044 | 0.528 | 0.303 | 0.116 | 0.067 | 0.040 | 0.042 | -1.8 |
| B1900+05 | 5 | 0.179 | 0.039 | 0.025 | 0.439 | 0.331 | 0.102 | 0.174 | 0.029 | 0.036 | -1.7 |
| B1900+06 | 6 | 0.352 | 0.061 | 0.043 | 0.402 | 0.212 | 0.083 | 0.058 | 0.023 | 0.026 | -2.2 |
| B1903+07 | 4 | 0.165 | 0.043 | 0.032 | 0.185 | 0.029 | 0.024 | 0.137 | 0.032 | 0.033 | -1.3 |
| B1904+06 | 4 | 0.141 | 0.178 | 0.061 | 0.131 | 0.060 | 0.044 | 0.246 | 0.075 | 0.103 | -0.7 |
| B1907+02 | 5 | 0.285 | 0.030 | 0.027 | 0.992 | 0.152 | 0.136 | 0.040 | 0.014 | 0.015 | -2.8 |
| B1907+03 | 5 | 0.215 | 0.056 | 0.047 | 1.448 | 0.821 | 0.476 | 0.190 | 0.030 | 0.028 | -1.8 |
| B1907+10 | 5 | 0.778 | 0.062 | 0.059 | 0.768 | 0.119 | 0.102 | 0.018 | 0.012 | 0.011 | -2.5 |
| B1911-04 | 5 | 1.249 | 0.105 | 0.098 | 0.497 | 0.039 | 0.037 | 0.060 | 0.012 | 0.012 | -2.6 |
| B1913+10 | 8 | 0.283 | 0.034 | 0.031 | 1.195 | 0.315 | 0.256 | 0.129 | 0.012 | 0.011 | -1.9 |
| B1915+13 | 8 | 0.533 | 0.215 | 0.143 | 0.380 | 0.184 | 0.082 | 0.120 | 0.064 | 0.063 | -1.8 |
| B1916+14 | 6 | 0.023 | 0.013 | 0.008 | 0.204 | 0.077 | 0.046 | 0.317 | 0.057 | 0.062 | -0.3 |
| B1919+21 | 10 | 1.190 | 0.065 | 0.067 | 0.490 | 0.043 | 0.042 | 0.011 | 0.005 | 0.005 | -2.6 |
| B1923+04 | 4 | 0.219 | 0.031 | 0.027 | 0.600 | 0.136 | 0.123 | 0.108 | 0.015 | 0.016 | -2.7 |
| B1929+10 | 19 | 5.355 | 0.830 | 0.895 | 0.078 | 0.022 | 0.013 | 0.163 | 0.015 | 0.013 | -1.6 |
| B1933+16 | 6 | 2.666 | 0.394 | 0.367 | 0.346 | 0.082 | 0.051 | 0.192 | 0.019 | 0.018 | -1.7 |
| B1935+25 | 6 | 0.112 | 0.053 | 0.032 | 0.153 | 0.027 | 0.021 | 0.282 | 0.048 | 0.054 | -0.7 |
| B1946+35 | 7 | 2.454 | 0.128 | 0.122 | 0.357 | 0.015 | 0.014 | 0.021 | 0.010 | 0.010 | -2.4 |
| B2000+40 | 8 | 1.009 | 0.030 | 0.043 | 0.235 | 0.015 | 0.009 | 0.003 | 0.008 | 0.002 | -2.2 |
| B2011+38 | 8 | 0.541 | 0.132 | 0.094 | 0.176 | 0.017 | 0.015 | 0.162 | 0.030 | 0.032 | $-1.9^b$ |
| B2020+28 | 12 | 2.511 | 1.159 | 0.724 | 0.116 | 0.021 | 0.016 | 0.159 | 0.031 | 0.032 | $-1.9^b$ |
| B2021+51 | 20 | 1.661 | 0.517 | 0.519 | 0.124 | 0.048 | 0.026 | 0.269 | 0.028 | 0.022 | $-1.5^b$ |
| B2022+50 | 8 | 0.015 | 0.003 | 0.003 | 2.014 | 0.675 | 0.751 | 0.544 | 0.034 | 0.034 | -0.8 |
| B2044+15 | 5 | 0.076 | 0.010 | 0.008 | 1.118 | 0.536 | 0.290 | 0.236 | 0.017 | 0.018 | -1.7 |
| B2045-16 | 11 | 2.235 | 0.341 | 0.347 | 0.238 | 0.030 | 0.028 | 0.069 | 0.013 | 0.012 | -2.1 |
| B2045+56 | 5 | 0.064 | 0.013 | 0.012 | 0.986 | 0.313 | 0.198 | 0.111 | 0.035 | 0.031 | -2.4 |
| B2053+36 | 6 | 0.265 | 0.018 | 0.015 | 0.566 | 0.070 | 0.061 | 0.161 | 0.012 | 0.013 | -1.9 |
| B2106+44 | 5 | 0.328 | 0.119 | 0.073 | 0.315 | 0.071 | 0.050 | 0.181 | 0.049 | 0.056 | -1.4 |
| B2110+27 | 6 | 0.257 | 0.030 | 0.027 | 0.675 | 0.170 | 0.203 | 0.079 | 0.012 | 0.013 | -2.2 |
| B2111+46 | 10 | 2.996 | 0.263 | 0.218 | 0.414 | 0.036 | 0.033 | 0.076 | 0.013 | 0.014 | -2.1 |
| B2148+52 | 7 | 0.080 | 0.007 | 0.006 | 1.074 | 0.697 | 0.381 | 0.333 | 0.013 | 0.014 | -1.3 |
| B2148+63 | 7 | 0.465 | 0.048 | 0.040 | 0.320 | 0.021 | 0.019 | 0.079 | 0.015 | 0.016 | -1.8 |
| B2154+40 | 7 | 1.392 | 0.517 | 0.303 | 0.292 | 0.074 | 0.053 | 0.128 | 0.040 | 0.047 | -1.6 |
| B2217+47 | 7 | 1.389 | 0.154 | 0.151 | 0.856 | 0.086 | 0.084 | 0.058 | 0.017 | 0.017 | -2.6 |
| B2227+61 | 5 | 0.178 | 0.018 | 0.016 | 0.703 | 0.065 | 0.060 | 0.072 | 0.020 | 0.021 | -2.6 |
| B2303+30 | 7 | 0.155 | 0.039 | 0.033 | 1.701 | 0.698 | 0.468 | 0.195 | 0.033 | 0.030 | -2.3 |
| B2310+42 | 10 | 1.072 | 0.099 | 0.087 | 0.495 | 0.063 | 0.055 | 0.093 | 0.011 | 0.012 | -1.9 |
| B2319+60 | 11 | 1.459 | 0.191 | 0.163 | 0.152 | 0.013 | 0.012 | 0.125 | 0.011 | 0.012 | $-2.1^b$ |
| B2324+60 | 7 | 0.618 | 0.153 | 0.177 | 0.168 | 0.026 | 0.018 | 0.044 | 0.044 | 0.029 | $-2.5^b$ |
| B2351+61 | 9 | 0.168 | 0.039 | 0.028 | 0.372 | 0.083 | 0.074 | 0.220 | 0.023 | 0.026 | -1.1 |

[]

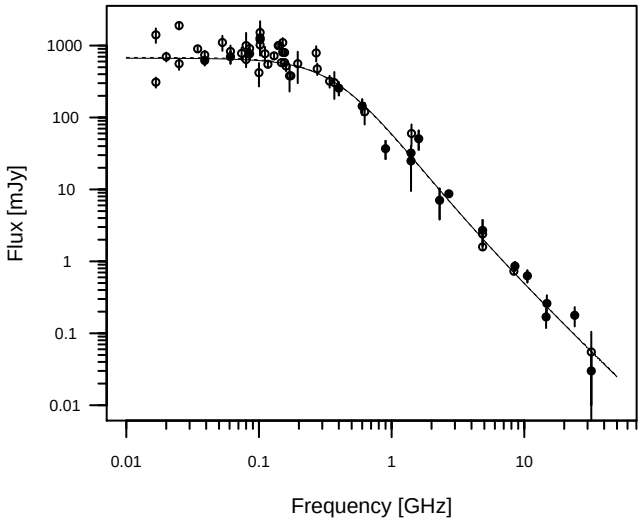



**Figure 1.** Fitted spectrum of PSR B1133+16. Black filled circles denote 19 flux measurement from Maron et al. (2000), while black open circles denote 41 additional points gathered in Krzeszowski et al. (2014). The fits are plotted with solid line and dashed line for Maron's data and Krzeszowski's datasets, respectively. Extending the original dataset of 19 with additional 41 measurements hasn't changed the fit (see sec. 3.1).

[ht]

**Table 2.** Comparison of the fitted values with the values in Löhmer et al. (2008) denoted with superscript $L$ for 12 pulsars.

| Pulsar | $S_0$ | $\tau$ | $n$ | $S_0^L$ | $\tau^L$ | $n^L$ |
|---|---|---|---|---|---|---|
| B0144+59 | 0.02 | 1.90 | 0.42 | 0.03 | 0.34 | 0.45 |
| B0329+54 | 10.08 | 0.26 | 0.08 | 22.00 | 0.16 | 0.07 |
| B0355+54 | 0.69 | 0.08 | 0.40 | 0.27 | 0.27 | 0.50 |
| B0628-28 | 2.70 | 0.55 | 0.10 | 3.09 | 0.62 | 0.11 |
| B0823+26 | 0.58 | 0.95 | 0.21 | 1.77 | 0.71 | 0.17 |
| B0950+08 | 12.62 | 0.30 | 0.06 | 7.68 | 0.42 | 0.12 |
| B1133+16 | 3.48 | 0.39 | 0.12 | 4.41 | 0.51 | 0.10 |
| B1706-16 | 0.28 | 0.84 | 0.28 | 0.40 | 0.91 | 0.27 |
| B1929+10 | 5.36 | 0.08 | 0.16 | 2.59 | 0.57 | 0.23 |
| B2020+28 | 2.51 | 0.12 | 0.16 | 1.61 | 0.12 | 0.28 |
| B2021+51 | 1.66 | 0.12 | 0.27 | 1.54 | 0.24 | 0.20 |
| B2022+50 | 0.02 | 2.01 | 0.54 | 0.03 | 1.77 | 0.48 |

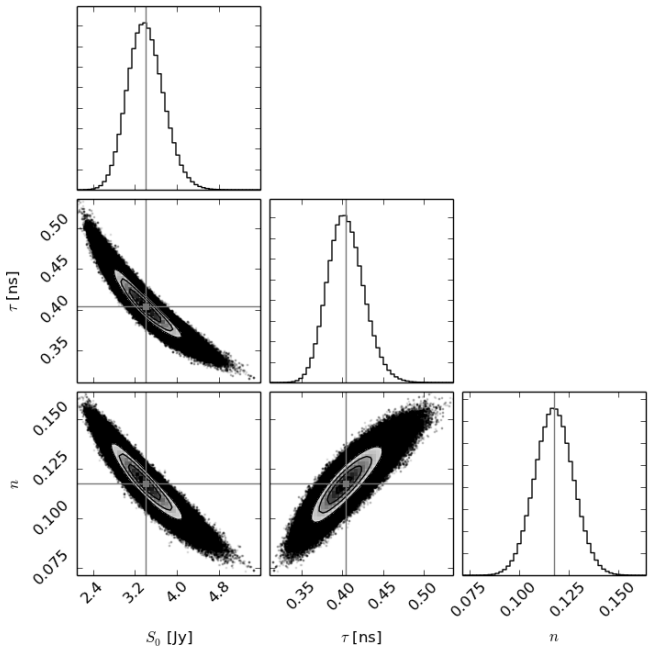



**Figure 2.** Triangle plot of distributions of fitted parameters (diagonal) and 2–d correlations between parameters for a number of MCMC walkers in parameter space of PSR B1133+16 extended data (60 measurements, see Fig. 1) spectrum fit. Solid vertical and horizontal lines denote most frequently occurring values of each parameter. The $16^{\text{th}}$ and $84^{\text{th}}$ percentile of each distribution are lower and upper uncertainties of each parameter estimation, respectively.

[]

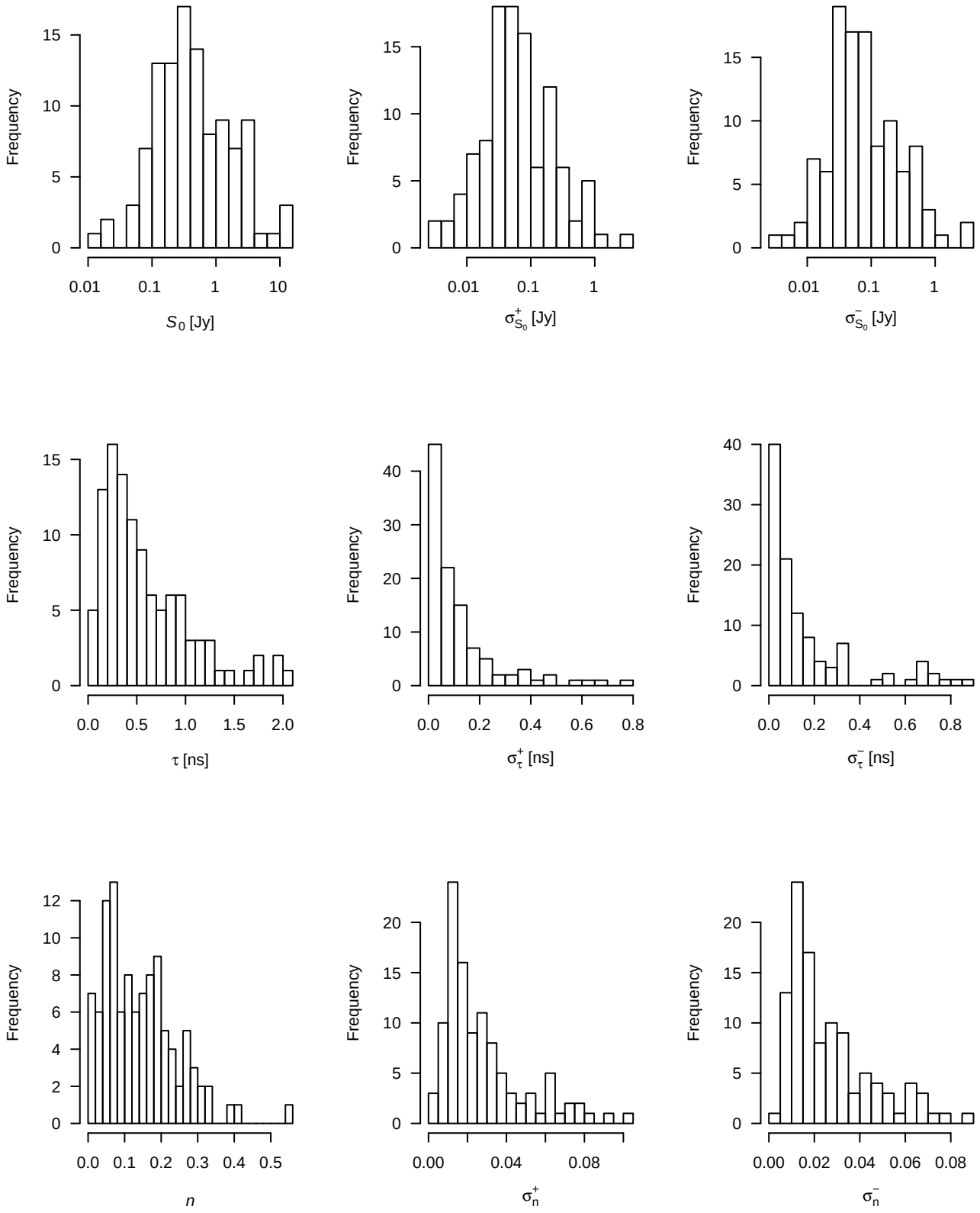



**Figure 3.** $S_0$, $\tau$ and $n$ and their upper and lower uncertainties distributions of spectra fitted to 108 pulsars flux measurements. Fifty percent of $S_0$, $\tau$ and $n$ values are between 0.17–1.20 Jy, 0.25–0.84 ns and 0.07–0.20 , respectively.

[]

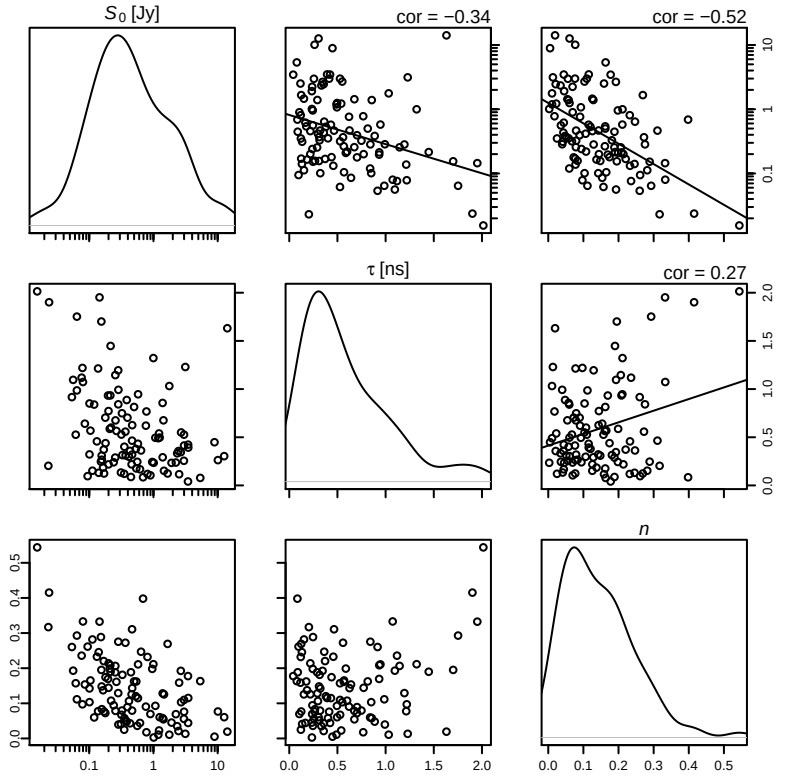



**Figure 4.** Density plots and correlations of fitted parameters $S_0$, $\tau$ and $n$. The first row shows the radio flux density distribution, the scatter plot and correlations between $\tau$ and $S_0$ as well as $n$ and $S_0$. The second row shows the scatter plot of $S_0$ versus $\tau$, the distribution of $\tau$ and the scatter plot and correlation between $n$ and $\tau$. The third row shows the scatter plots of $S_0$ versus $n$ ans $\tau$ versus $n$ as well as the distribution of $n$. Pearson's correlation indices are printed over upper corner panels. There is a strong negative correlation between $\log S_0$ and $n$.

[]

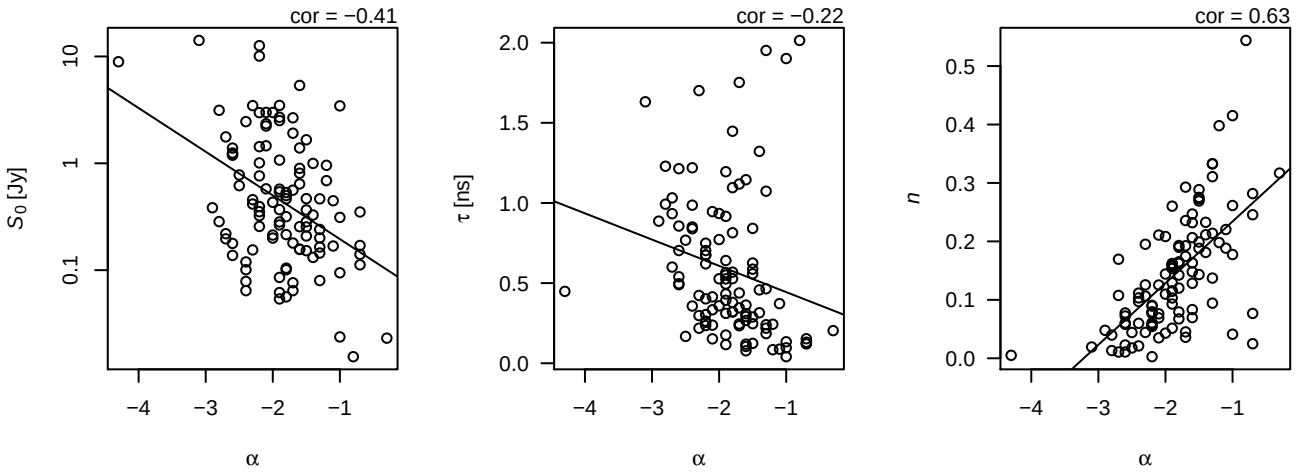



**Figure 5.** Correlation plots of the parameters $S_0$, $\tau$ and $n$ obtained from our fit with the spectral indices $\alpha$ of single power–law fits from Maron et al. (2000). There are no obvious correlations between $S_0$ and $\tau$ with $\alpha$. However, there is a strong positive relationship between $n$ and $\alpha$ with Pearson's correlation index of 0.63.

## 4 SUMMARY AND CONCLUSIONS

The main conclusion of our work is that the pulsar radio spectrum can be well described with flicker noise model proposed by Löhmer et al. (2008) for a high number of pulsars. The crucial constraint on the quality of fitting the flicker noise spectrum model is the coverage of frequency space. There should be flux measurements at low ($<$ 200 MHz) and high ($>$ 1 GHz) frequencies to obtain reliable parameter estimates. We have flux measurements for many more pulsars but they lack either low or high frequency data. We are planning to extend Maron's database with published measurements and new observations. In the best case it will almost double our sample up to 281 pulsars for our future study.

Maron et al. (2000) fitted spectrum for flux measurements above 300 MHz even if they had data points at lower frequencies because of so called low–frequency turn–over, which can not be reasonably represented with power–law model. In our work we took into account all the points, including those below 300 MHz gathered by Maron et al. (2000) and successfully fitted the flicker noise spectrum model. The most outstanding example of extension of the data is the case of PSR B1133+16, which justifies application of Löhmer's model, that describes pulsar radio spectrum in wide frequency range from 17 MHz up to 32 GHz. To reproduce more complex shape of a pulsar spectrum with power–laws one should combine three or more of them to get a reasonable fit. This approach is artificial and most likely non-physical. It seems that flicker noise model has an advantage over a power–law model and also over broken power–law. Not only does it describe the spectra in higher frequency range with only two parameters, not counting scaling factor $S_0$, but it also shows a smooth transition from flat to steep behaviour at lower and higher frequencies, respectively. Based on our dataset of 108 pulsars we found that fifty percent of $S_0$, $\tau$ and $n$ values are between 0.17–1.20 Jy, 0.25–0.84 ns and 0.07–0.20, respectively.

We conclude that there is a strong negative correlation between the flicker noise spectrum model parameters $\log S_0$ and $n$, which may indicate a selection bias as high frequency detections would be improbably for weak steep spectrum sources, and a strong positive relationship between $n$ and the power–law spectral index $\alpha$. The latter implies, that the physical meaning of both parameters must be similar. The flicker noise spectrum behaves in the similar manner as the power–law at higher frequencies and is able to describe the data at lower frequencies at the same time, which is another advantage of this model.

Furthermore, in our study we have not found any correlations of the model parameters $S_0$, $\tau$ and $n$ with pulsar physical properties like period, period derivative, age, rotational energy loss, magnetic field on surface or dispersion and rotation measures.

## ACKNOWLEDGEMENTS

This work has been supported by Polish National Science Centre grants DEC-2011/03/D/ST9/00656 (KK, AS) and DEC-2012/05/B/ST9/03924 (OM). Data analysis and figures were partly prepared using R (R Core Team 2013). We want to thank prof. Krzysztof Goździewski from CA UMK (Toruń, Poland) for very useful and fruitful discussion on the MCMC application to fitting non–linear models to data.

## REFERENCES

Andrae R., Schulze-Hartung T., Melchior P., 2010, ArXiv e-prints
Foreman-Mackey D., Hogg D. W., Lang D., Goodman J., , 2012, emcee: The MCMC Hammer
Gelfand A. E., Smith A. F., 1990, Journal of the American Statistical Association, 85, 398
Han J. L., Demorest P. B., van Straten W., Lyne A. G., 2009, ApJS, 181, 557
Izvekova V. A., Kuzmin A. D., Malofeev V. M., Shitov I. P., 1981, Ap&SS, 78, 45
Krzeszowski K., Maron O., Słowikowska A., Dyks J., Jessner A., 2014, MNRAS, 440, 457
Löhmer O., Jessner A., Kramer M., Wielebinski R., Maron O., 2008, A&A, 480, 623
Lorimer D. R., Yates J. A., Lyne A. G., Gould D. M., 1995, MNRAS, 273, 411
Malofeev V. M., Gil J. A., Jessner A., Malov I. F., Seiradakis J. H., Sieber W., Wielebinski R., 1994, A&A, 285, 201
Maron O., Kijak J., Kramer M., Wielebinski R., 2000, A&AS, 147, 195
R Core Team 2013, R: A Language and Environment for Statistical Computing. R Foundation for Statistical Computing, Vienna, Austria
Seiradakis J. H., Gil J. A., Graham D. A., Jessner A., Kramer M., Malofeev V. M., Sieber W., Wielebinski R., 1995, A&AS, 111, 205
Sieber W., 1973, A&A, 28, 237

This paper has been typeset from a TEX/ LATEX file prepared by the author.